

TiO₂ Synthesis Inspired by Biomineralization: Control of Morphology, Crystal Phase, and Light-Use Efficiency in a Single Process

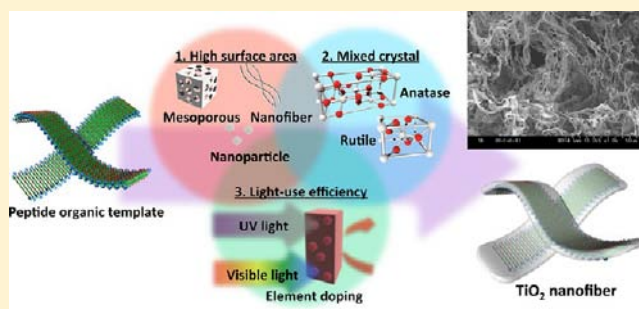
Takayuki Nonoyama,[†] Takatoshi Kinoshita,^{*,†} Masahiro Higuchi,[‡] Kenji Nagata,[‡] Masayoshi Tanaka,[†] Kimiyasu Sato,[§] and Katsuya Kato^{*,§}

[†]Department of Frontier Materials and [‡]Department of Materials Science and Engineering, Graduate School of Engineering, Nagoya Institute of Technology, Gokiso-cho, Showa-ku, Nagoya, Aichi 466-8555, Japan

[§]National Institute of Advanced Industrial Science and Technology, 2266-98 Anagahora, Shimo-Shidami moriyama-ku, Nagoya, Aichi 463-8560, Japan

S Supporting Information

ABSTRACT: Hydroxyapatite is mineralized along the long axis of collagen fiber during osteogenesis. Mimicking such biomineralization has great potential to control inorganic structures and is fast becoming an important next-generation inorganic synthesis method. Inorganic matter synthesized by biomineralization can have beautiful and functional structures that cannot be created artificially. In this study, we applied biomineralization to the synthesis of the only photocatalyst in practical use today, titanium dioxide (TiO₂). The photocatalytic activity of TiO₂ mainly relates to three properties: morphology, crystal phase, and light-use efficiency. To optimize TiO₂ morphology, we used a simple sequential peptide as an organic template. TiO₂ mineralized by a β -sheet peptide nanofiber template forms fiber-like shapes that are not observed for mineralization by peptides in the shape of random coils. To optimize TiO₂ crystal phase, we mineralized TiO₂ with the template at 400 °C to transform it into the rutile phase and at 700 °C to transform it into a mixed phase of anatase and rutile. To optimize light-use efficiency, we introduced nitrogen atoms of the peptide into the TiO₂ structure as doped elemental material during sintering. Thus, this biomineralization method enables control of inorganic morphology, crystal phase, and light-use efficiency in a single process.



■ INTRODUCTION

Titanium dioxide (TiO₂) is of interest because of its wide range of applications as a photocatalyst, printing photoconductor, catalyst support, solar battery component, and more. In particular, because TiO₂ is the only substance in practical use today as a photocatalyst, numerous related research reports and patents have been published in the past decades.^{1–5} Among major findings, particularly important is that the photocatalytic activity of TiO₂ depends strongly on three properties: morphology (surface area),^{6–8} crystal phase,^{9–11} and light-use efficiency.^{12,13}

TiO₂ exhibits three crystal phases. The most catalytically active phase is anatase, the most stable phase is rutile,¹⁴ and the third phase is brookite.^{15,16} Catalytic activity is even higher when TiO₂ contains a mixture of phases rather than just a single phase; in particular, a mixture of anatase and rutile phases.^{17–19} The metastable anatase and brookite phases are transformed into the more stable rutile phase by calcination at high temperature, making it difficult to produce mixed crystal phases of anatase and rutile by a single sintering process.

In general, pure TiO₂ absorbs only ultraviolet light²⁰ and does not use sunlight efficiently. Previous studies report that element-doped TiO₂ exhibits better visible-light absorbance and

higher activity than pristine TiO₂.^{21,22} In particular, nitrogen-doped TiO₂ appears to use visible light efficiently.²³

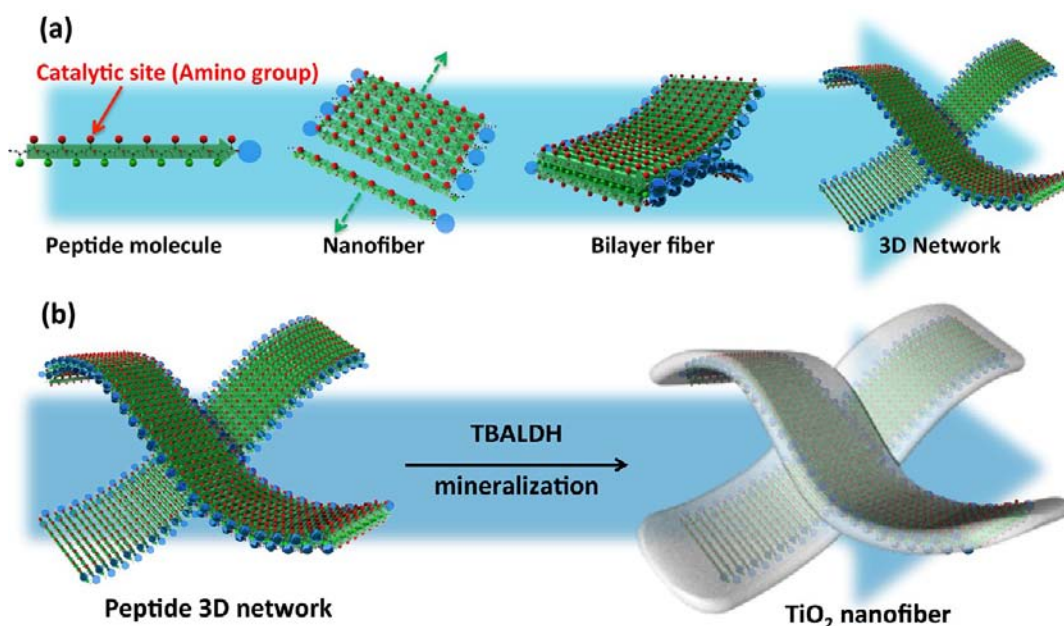
Our goal in this study was to devise a single process for preparing TiO₂ material that contains both a favorable mixture of crystal phases for optimizing catalytic activity and favorable doping for optimizing light-use efficiency. To this end, we considered the concept of mineralization with self-assembled biomolecules, that is, biomineralization. Biomineralization is a biomimetic and environmental friendly synthesis process that proceeds at ordinary temperature and pressure. We have previously used biomineralization to synthesize inorganic matter.^{24–26} Inorganic matter synthesized by biomineralization can have intricate and functional structures that cannot be created artificially.^{27,28} During biomineralization, a surface functional group from an organic substance catalyzes and mineralizes an inorganic substance.^{29,30} The morphology and crystal phase of the produced mineral are controlled by the organic substance via the so-called “template effect”.

In this study, we describe the process by which anionic titanium complex is captured by an amino group on a lysine

Received: December 5, 2011

Published: May 11, 2012

Scheme 1. (a) Hierarchical Self-Assembly of β -Sheet Peptide into a 3D Nanofiber Network^a; (b) TiO₂ Mineralization Occurs at the Surface of the Amino Group Side of the Peptide Nanonetwork^b



^aThe β -strand peptides self-assemble into antiparallel β -sheet conformations. Then, the leucine sides of the nanofiber pack face-to-face via hydrophobic interaction. The bilayer nanofibers intertangle hierarchically and form a 3D nanonetwork.

^bThe amino group captures anionic TBALDH, and then mineralization (heterogeneous nucleation) starts on the peptide surface.

side chain causing nitrogen from the amino group to closely approach the mineralized TiO₂, where it can be incorporated in the TiO₂ structure during sintering. On the basis of this description, we speculated that biomineralization may be an ideal synthetic method for controlling morphology, crystal phase, and light-use efficiency all in a single process.

For this study, we used the following materials. For the titanium source, we used anionic titanium bis(ammonium lactato) dihydroxide (TBALDH). For hydrophilic amino acid that is to capture the TBALDH anion, we used cationic lysine residues having an amino group on the side chain. For the catalytic organic template, we started with a simple sequential peptide made to assume a β -sheet conformation by the presence of alternating hydrophilic and hydrophobic amino acids.^{31–33} To prevent aggregation of the β -sheet peptide and enhance peptide solubility in water, we introduced polyethylene glycol (PEG, degree of polymerization = 70) at the C-terminus of the seeding peptide. Accordingly, we designed (leucine-lysine)₈-PEG₇₀ ((LK)₈-PEG₇₀) as the organic catalytic template for TiO₂ mineralization. In a basic aqueous environment, (LK)₈-PEG₇₀ peptide spontaneously self-assembles to a single nanofiber that self-assembles when driven by the hydrophobicity of the exposed leucine side chains via hydrophobic interactions (Scheme 1). Bilayer nanofibers hierarchically intertangle and form a three-dimensional (3D) nanonetwork. We expect such a nanonetwork should enable us to control the morphology and crystal phase of mineralized inorganic matter in a manner similar to that observed during osteogenesis *in vivo*.

RESULTS AND DISCUSSION

Template Effect Caused by Peptide. First, we investigated the effect of amino acid sequence on TiO₂ mineralization. We stirred aqueous solutions containing (LE)₈-PEG₇₀, (LELK)₄-PEG₇₀, or (LK)₈-PEG₇₀ (2 mg/200 μ L, pH 11.0) with 20 μ L of 50 mM TBALDH at 70 °C for 48 h. Figure 1 shows scanning electron microscopy (SEM) images of TiO₂ mineralized on the peptide template. Nanofiber-shaped TiO₂ is observed in the (LK)₈-PEG₇₀ system; it presumably forms when the cationic titanium complex is captured, concentrated by the amino group on the side chain of lysine, and then nucleated (Figure 1a). In contrast, TiO₂ is not observed in the (LE)₈-PEG₇₀ system (Figure S1a [Supporting Information (SI)]), and only an infinitesimal precipitate is observed in the (LELK)₄-PEG₇₀ system (Figure S1b [SI]). Therefore, only the cationic functional group from the titanium complex enables efficient mineralization of the TiO₂ in the same complex.

Next, we investigated the template effect on TiO₂ shape by examining TiO₂ mineralization using templates of different peptides with different secondary structures: (LK)₈-PEG₇₀ and, for a control, commercially available polylysine (M_w = 1000–5000, Sigma Aldrich). Figure 2 shows circular dichroism (CD) spectra of the secondary structures of (LK)₈-PEG₇₀ and polylysine at room temperature and at 70 °C. At both temperatures, (LK)₈-PEG₇₀ and polylysine show stable β -sheet and random coil conformations, respectively, in a pH 11.0 aqueous environment. We already showed that mineralization in the presence of (LK)₈-PEG₇₀ as an organic template gives the desired nanofibrous TiO₂. In contrast, mineralization in the presence of polylysine as an organic template gives bulky precipitates under the same conditions (Figure 1b). Therefore,

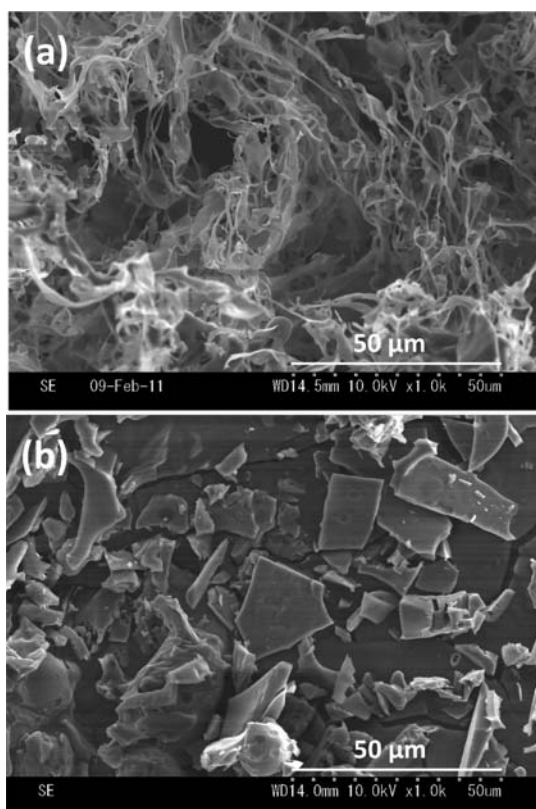


Figure 1. SEM images of TiO_2 . (a) Mineralized by $(\text{LK})_8\text{-PEG}_{70}$. (b) Mineralized by polylysine.

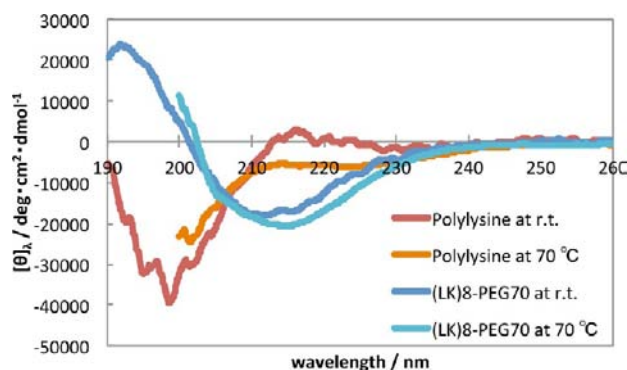


Figure 2. CD spectra of polylysine and $(\text{LK})_8\text{-PEG}_{70}$, taken at room temperature and at $70\text{ }^\circ\text{C}$.

to achieve a nanofibrous TiO_2 morphology, we require the well-controlled peptide secondary structure present in $(\text{LK})_8\text{-PEG}_{70}$. Henceforward, we abbreviate TiO_2 mineralized by $(\text{LK})_8\text{-PEG}_{70}$ and polylysine as LKTiO_2 and pKTiO_2 , respectively.

Rutile Formation During Low-Temperature Sintering.

Unfortunately, both LKTiO_2 and pKTiO_2 are amorphous (data not shown), as expected for TiO_2 synthesized in an aqueous environment.³⁴ To force crystallization, we sintered TiO_2 /peptide composites and titanium complex at $400\text{ }^\circ\text{C}$ for 4 h. The morphology of LKTiO_2 collapses slightly during sintering because organic peptide matter and coordinate lactate outburn during calcination, but the nanofiber structure remains (Figure S2 [SI]). Figure 3 shows X-ray diffraction (XRD) profiles of TiO_2 (as LKTiO_2 and pKTiO_2) after sintering and of the TiO_2 source. The pKTiO_2 consists mainly of mixed anatase and brookite phases, which agrees with the sintering result for

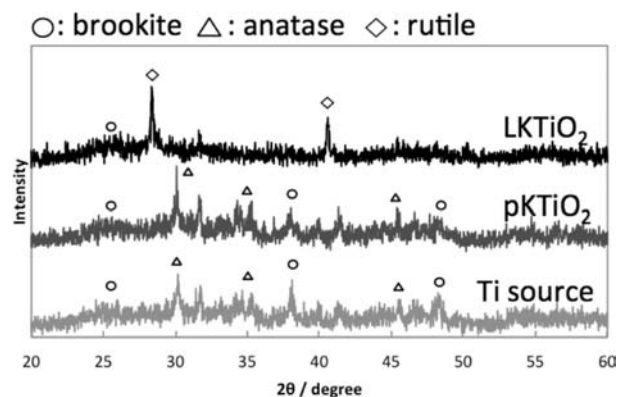


Figure 3. XRD profiles of LKTiO_2 , pKTiO_2 , and Ti source, each sintered at $400\text{ }^\circ\text{C}$. Symbols: circle = brookite phase, triangle = anatase phase, and rhomboid = rutile phase.

TBALDH only. Interestingly, LKTiO_2 has sharp peaks at 27 and 42° , attributable to the rutile phase. In general, the rutile phase, the most stable crystal phase of TiO_2 , is obtained by calcination at $>900\text{ }^\circ\text{C}$.¹⁹ We believe that an important factor in our obtaining it at lower temperature is the spatial position of the titanium atom achieved using the β -sheet peptide template. We speculate that the amino group of the lysine residue captures the titanium complex, confining the titanium-atom position on the lysine side chain in the earliest stage; mineralization, which is a heterogeneous nucleation process, then starts at the lysine side chain. The distances between amino groups along a fiber's long and short axes in β -sheet conformation are 4.7 and 7.0 \AA , respectively. The titanium-atom positions on the anatase phase and rutile phase a -face are superimposed on the amino-group positions in the β -sheet peptide (Figure 4b,c). In the case of anatase, the four titanium-atom positions at the corners of two unit cells almost fit with the amino group positions in the directions of both the fiber's long and short axes, but the titanium-atom position on the inside of the unit cell does not fit with the amino group position. In contrast, in the case of rutile, the titanium-atom positions in the unit cell almost fit in the direction of the fiber's long axis; however, in the direction of the fiber's short axis, the titanium atom interval in a single cell differs from the amino-group interval more than that for anatase, but the gap between the titanium atom interval for rutile and the amino group interval almost resolves every two unit cells. Moreover, in the earliest stage, all amino groups essentially capture the anionic titanium complex because of charge balance; therefore, from the viewpoint of atomic position, the rutile phase might form more easily than the anatase phase. We did not consider the c -face of anatase and rutile because the titanium-atom position on the c -face is less consistent with the amino-group position than that on the a -face for both anatase and rutile. Therefore, the spatial positions of the functional groups in the β -sheet peptide's side chain are strictly controlled (Figure 4a). In contrast, polylysine assumes a random coil conformation during mineralization, and titanium atoms are positioned randomly.

We sintered amorphous LKTiO_2 and investigated the thermal dependence of the resulting crystal phase. Figure 5a shows XRD profiles of LKTiO_2 after sintering at various temperatures. LKTiO_2 sintered at $\leq 200\text{ }^\circ\text{C}$ does not form a crystal phase. The LKTiO_2 sintered at $400\text{ }^\circ\text{C}$ forms only the rutile phase, and LKTiO_2 sintered at $700\text{ }^\circ\text{C}$ forms coexisting anatase and rutile phases. Therefore, amorphous TiO_2

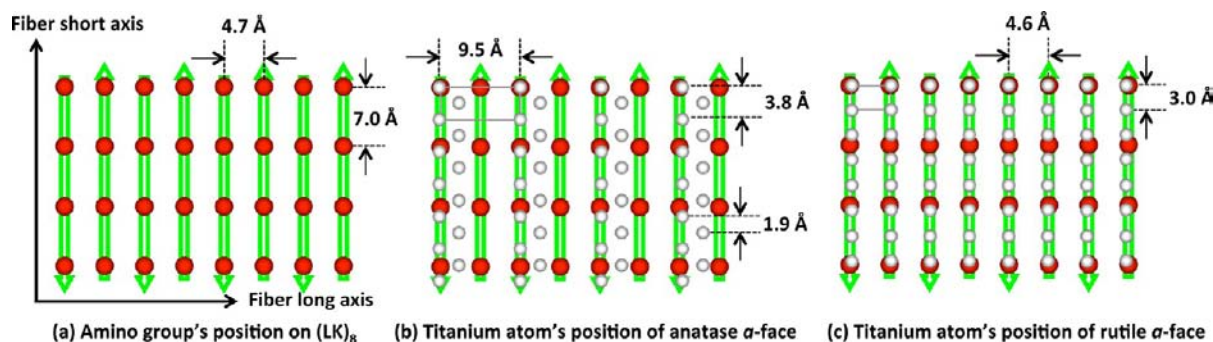


Figure 4. (a) Amino group positions (spatial arrangement) on the surface of a β -sheet peptide nanofiber. (b) Ti-atom positions on the anatase phase a -face, superimposed on (a). (c) Ti-atom positions on the rutile phase a -face, superimposed on (a).

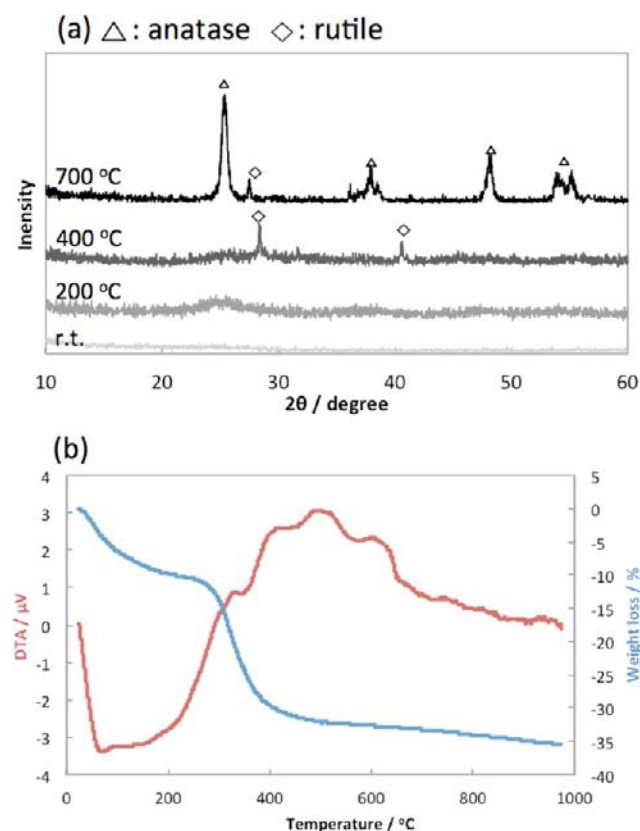


Figure 5. (a) XRD profiles of $LKTiO_2$ sintered at room temperature (i.e., unsintered), 200, 400, and 700 °C. Symbols: triangle = anatase phase, rhomboid = rutile phase. (b) TGA/DTA curves for $LKTiO_2$.

transforms partly to the rutile phase at 400 °C and fully to the anatase phase at 400–700 °C. Thinking that this phase transition from amorphous to anatase is normal for calcination, we investigated the phase-transitional points of anatase and rutile by thermogravimetric analysis/differential thermal analysis (TGA/DTA). Figure 5b shows the TGA/DTA profile of $LKTiO_2$. At 300 °C, the exothermic peak indicates combustion of organic matter because of the intensive weight loss at this temperature. At 400 °C, the next peak indicates the phase transition from amorphous to rutile. At 500–600 °C, the final peak indicates the phase transition from amorphous to anatase.

We investigated the detailed structure of TiO_2 nanofiber sintered at 700 °C by high-resolution transmission electron microscopy (TEM) and selected-area electron diffraction

(SAED). Figure 6a shows TEM images of $LKTiO_2$ nanofiber sintered at 700 °C. The nanofiber consists of an assembly of

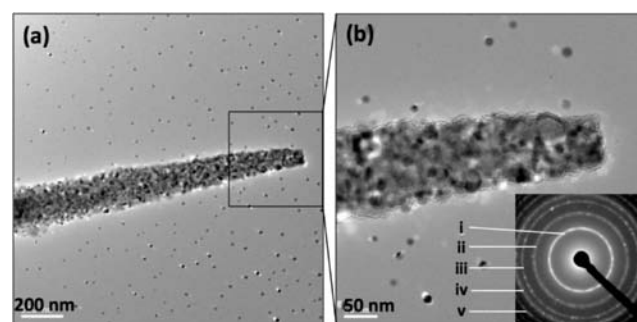


Figure 6. (a) High-resolution TEM images of $LKTiO_2$ sintered at 700 °C. (b) Zoom image of (a). (Inset) SAED shows diffraction rings of (i) anatase $A(101)$, rutile $R(120)$, (ii) $A(004)$, $R(111)$, (iii) $A(105)$, $A(211)$, $R(211)$, $R(220)$, (iv) $A(200)$, and (v) $R(301)$.

cubic nanocrystals. Figure 6b (inset) shows SAED images indicating that both anatase and rutile form isotropically; therefore, mixed crystals exist homogeneously. From the viewpoints of atomic position and phase transition, the amorphous phase, which can transform to the rutile phase, has a component in which the Ti-atom positions of rutile fit with amino group positions in the β -sheet peptide. Therefore, the anatase phase forms at the interspace between rutile phases, and two crystal phases coexist on a nanoscale level.

We investigated the elemental composition of the $LKTiO_2$ nanofiber by energy-dispersive X-ray spectroscopy (EDX). Figure 7 shows a scanning TEM (STEM) image and several elemental mapping images. Not only the titanium and oxygen mapping images but also the nitrogen mapping image conform to the STEM image. Organic matter completely outburns at 700 °C. Therefore, nitrogen is clearly doped in the TiO_2 structure. Such nitrogen doping is expected to increase light-use efficiency as it relates to photocatalytic activity.

Photocatalytic Activity. Finally, we investigated the photocatalytic activity of mineralized TiO_2 as compared with that of the commercially available Degussa P25 TiO_2 powder.

We investigated the light-absorbance capability of mineralized TiO_2 powder by ultraviolet/visible (UV/visible) spectroscopy. Figure 8a shows UV/visible spectra of $LKTiO_2$ after sintering at various temperatures and of $pKTiO_2$ after sintering at 700 °C. $LKTiO_2$ sintered at <400 °C absorbs only UV radiation, because at that temperature peptide does not outburn completely and nitrogen does not become doped in the TiO_2

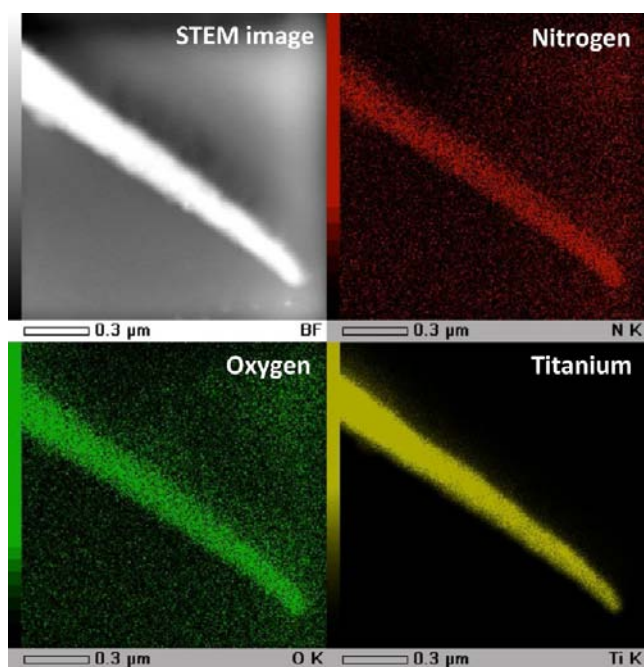


Figure 7. EDX mapping images of LKTiO₂. The titanium, oxygen, and nitrogen mapping images all agree well with the STEM image. Nitrogen is doped in the TiO₂ structure.

structure. In contrast, both LKTiO₂ and pKTiO₂ sintered at 700 °C absorb from the UV to the visible range because of nitrogen doping.

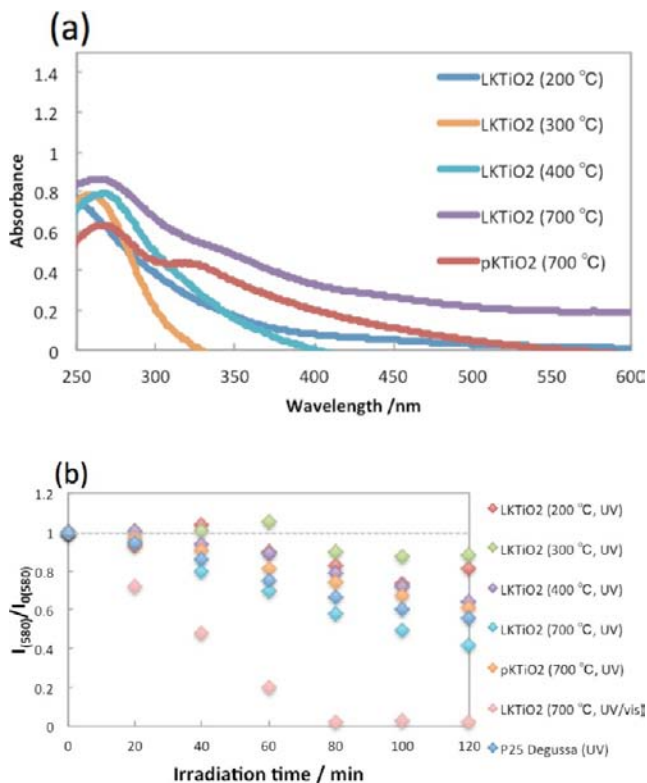


Figure 8. (a) UV spectra of LKTiO₂ sintered at 200, 300, 400, and 700 °C, and of pKTiO₂ sintered at 700 °C. (b) Photodegradation of rhodamine B, measured by fluorescence spectroscopy.

We investigated photocatalytic activity using rhodamine B. A 1.0 mg sample of TiO₂ powder was dispersed in 1 mL of 1.0×10^{-5} M rhodamine B aq solution (pH 7.0), and the suspension was irradiated for 2 h. Figure 8b shows photolytic degradation plots of rhodamine B (data recorded every 20 min). The vertical scale, $I_{(580)}/I_{0(580)}$, is the fluorescence intensity ratio of 580 nm maximum peak after and before irradiation. For irradiation with only UV light (365 nm), LKTiO₂ sintered at 200 and 300 °C exhibits very little photocatalytic activity. Photocatalytic activity clearly increases with sintering temperature.

In addition to LKTiO₂, pKTiO₂ also exhibits photocatalytic activity. We speculate that the difference in activity level between LKTiO₂ and pKTiO₂ is due to differences in surface area and crystal phase. The morphologies of LKTiO₂ and pKTiO₂ differ; the former is a 3D nanofiber network with a greater surface area, and the latter is a bulk form with less surface area. The crystal phases of LKTiO₂ and pKTiO₂ also clearly differ; LKTiO₂ exhibits coexisting rutile and anatase phases after sintering at 700 °C, but pKTiO₂ does not exhibit a rutile phase.

As noted previously, photocatalytic activity is generally higher for mixed-crystal than for single-crystal TiO₂. Photocatalytic activity is similar for the control sample Degussa P25 TiO₂ powder, pKTiO₂, and LKTiO₂ sintered at 700 and 400 °C, respectively. These data suggest that LKTiO₂ exhibits higher photocatalytic activity than pKTiO₂. Moreover, rhodamine B aq solution containing LKTiO₂ sintered at 700 °C, after irradiation with UV/visible light (365–600 nm), exhibits the highest photocatalytic activity observed for this study: rhodamine B degrades completely at 80 min and completely loses its pink color at 120 min (Figure S3 [SI]). Therefore, LKTiO₂ sintered at 700 °C and doped with nitrogen readily absorbs visible light and exhibits efficient photocatalytic activity. After 10 repetitions of the rhodamine B degradation test (Figure S4 [SI]), the catalytic activity of TiO₂ prepared by mineralization does not diminish, suggesting that it is stable and can be used repeatedly. This high activity of LKTiO₂ sintered at 700 °C is achieved by the synergistic effect of surface area, mixed-crystal phases, and elemental doping.

CONCLUSION

We synthesized TiO₂ by a biomineralization-inspired method that enables simultaneous control of TiO₂ morphology, crystal phase, and light-use efficiency in a single process. TiO₂ morphology is effectively controlled by the use of a designed peptide template. We used a nanofiber-like shape as the template in this study, but it should be possible to mineralize material having various shapes such as helix, tube sheet, or sphere using corresponding morphological organic matter as a template.

Our most interesting result is that we achieved the low-temperature synthesis of the rutile phase of TiO₂. We speculate that the positional relationship of atom and functional group before mineralization is important because LKTiO₂ and pKTiO₂ differ only in the secondary structure of their peptide. Mineralization (a heterogeneous nucleation process) initially occurs at the functional group of the organic matter; therefore, we think that the ion-capturing functional group's position is important and affects the subsequent growth of the mineralized inorganic matter.

We are continuing our efforts to clarify the epitaxial relationship between the organic and inorganic interfaces.

The constitutive nitrogen of peptide is successfully introduced into the TiO₂ structure during sintering; as a result, light-use efficiency is improved. Other types of organic matter commonly contain the necessary constitutive nitrogen, but peptide is particularly suitable for use as an organic template because it can control not only light-use efficiency but also morphology and mineral crystal phase. We believe that such inorganic syntheses inspired by living systems have great potential for the creation of novel functional inorganic materials and organic/inorganic hybrid materials.

EXPERIMENTAL SECTION

Peptide Synthesis. The hydrophilic/hydrophobic alternating peptide was synthesized by combinatorial solid-phase peptide synthesis. Fmoc-amino acids (Fmoc: 9-fluorenylmethoxycarbonyl) were polymerized in the order of the sequence on PEG₇₀ preloaded resin (Tenta-Gel PAP). To cap the N-terminal amino group with an acetyl group, the resin was stirred in a mixture of acetic anhydride and pyridine (v/v 1/2) for 4 h. To remove all side-chain protective groups and detach the peptide-PEG copolymer from the resin, the resin was added to a cocktail of 95 vol % trifluoroacetic acid (TFA) containing 2 vol % ethanedithiol, 2 vol % water, and 1 vol % thioanisole. Then the peptide-PEG-containing cocktail was dropped into diethylether, and the precipitated peptide was recovered and lyophilized.

The synthesized peptides were checked by matrix-assisted laser desorption/ionization time-of-flight mass spectrometry (Figure S5 [SI]).

Titanium Dioxide Mineralization. Mineralization was performed on TiO₂ with four peptides: (LK)₈-PEG₇₀, (LELK)₄-PEG₇₀, (LE)₈-PEG₇₀, and polylysine. A 2.0 mg sample of peptide was dissolved in 10 mL of distilled water, and the solution was adjusted to pH 11.0 with sodium hydroxide. Then 20 μL of 50 mM TBALDH (Sigma Aldrich) aq solution as the titanium source was mixed with the peptide solution. The mixture was stirred for 48 h at 70 °C. After mineralization, the precipitate was recovered and rinsed by centrifugal separation.

Sintering. TiO₂ mineralized by the peptide was sintered under the following conditions: rate of temperature increase, 1 °C/min; sintering time, 4 h; sintering temperatures, 200, 300, 400, and 700 °C. TGA/DTA was measured on a thermogravimetric analysis system (RTG320U, Seiko Instruments) from 20 to 1000 °C at a rate of 10 °C/min.

Determination of Peptide Secondary Structures. (LK)₈-PEG₇₀ and polylysine secondary structures were determined by spectropolarimeter (J-820K, Jasco). 1.0 × 10⁻⁵ M peptide aq solution (pH 11.0) was added to a quartz cell (optical length 1 mm). CD spectra were recorded from 190 to 260 nm at room temperature and at 70 °C.

Determination of TiO₂ Morphology and Crystal Phase. Morphology was determined by examination of images obtained by FE-SEM (S4300, Hitachi) and TEM (JEM-z2500, JEOL). Crystal phases were determined by XRD (RINT2000/PC, Rigaku).

Determination of TiO₂ Photocatalytic Activity. UV spectra of various TiO₂ samples were measured at room temperature on a UV/visible spectrometer (V550, Jasco). A 1 mg sample of TiO₂ powder was dispersed in 1 mL of distilled water. Spectra were recorded from 200 to 600 nm.

The photocatalytic activity of synthesized TiO₂ was investigated by dye degradation under UV or UV/visible light irradiation (wavelengths 365 and 365–600 nm, respectively). A 1 mg sample of TiO₂ powder was dispersed in 1 mL of 1.0 × 10⁻⁵ M rhodamine B aq solution (pH 7.0). Light from a mercury lamp (525 W) was used to irradiate the solution from a distance of 3 cm. Degradation of rhodamine B was detected by fluorescent spectroscopy (FP-777, Jasco).

ASSOCIATED CONTENT

Supporting Information

SEM images of TiO₂ mineralized by (LE)₈-PEG₇₀ and (LELK)₄-PEG₇₀. SEM image of LKTiO₂ sintered at 400 °C.

Rhodamine B degradation by LKTiO₂ sintered at 700 °C. Repeat test of photocatalytic activity of LKTiO₂ sintered at 700 °C. MALDI-TOF-MS spectra of peptides. This material is available free of charge via the Internet at <http://pubs.acs.org>.

AUTHOR INFORMATION

Corresponding Author

kinoshita.takatoshi@nitech.ac.jp; katsuya-kato@aist.go.jp

Notes

The authors declare no competing financial interest.

ACKNOWLEDGMENTS

We acknowledge the support of the Institute of Ceramics Research and Education (ICRE) administered by the Nagoya Institute of Technology (Prof. T. Kasuga and Prof. Y. Iwamoto). This work is partly supported by Grant-in-Aid for Scientific Research (C) No.23560925 from the Japan Society for the Promotion of Science (JSPS).

REFERENCES

- (1) Fujishima, A.; Honda, K. *Nature* **1972**, *238*, 37–38.
- (2) Regan, B. O.; Grätzel, M. *Nature* **1991**, *353*, 737–740.
- (3) Mills, A.; Hunte, S. L. *J. Photochem. Photobiol., A* **1997**, *108*, 1–35.
- (4) Cozzoli, P. D.; Kornowski, A.; Weller, H. *J. Am. Chem. Soc.* **2003**, *125*, 14539–14548.
- (5) Chen, X.; Mao, S. S. *Chem. Rev.* **2007**, *107*, 2891–2959.
- (6) Antonelli, D. M.; Ying, Y. J. *Angew. Chem., Int. Ed. Engl.* **1995**, *34*, 2014–2017.
- (7) Ying, Y. J. *AIChE J.* **2000**, *46*, 1902–1906.
- (8) Yu, J. C.; Zhang, L.; Zheng, Z.; Zhao, J. *Chem. Mater.* **2003**, *15*, 2280–2286.
- (9) Hoffmann, M. R.; Martin, S. T.; Choi, W.; Bahnemann, D. W. *Chem. Rev.* **1995**, *95*, 69–96.
- (10) Ding, Z.; Lu, G. Q.; Greenfield, P. F. *J. Phys. Chem. B* **2000**, *104*, 4815–4820.
- (11) Meulen, T. V. D.; Mattson, A.; Österlund, L. *J. Catal.* **2007**, *251*, 131–144.
- (12) Wang, J.; Tafen, D. N.; Lewis, J. P.; Hong, Z.; Manivannan, A.; Zhi, M.; Li, M.; Wu, N. *J. Am. Chem. Soc.* **2009**, *131*, 12290–12297.
- (13) Yu, H.; Irie, H.; Hashimoto, K. *J. Am. Chem. Soc.* **2010**, *132*, 6898–6899.
- (14) Shannon, R. D.; Pask, J. A. *J. Am. Ceram. Soc.* **1965**, *48*, 391–398.
- (15) Maruska, H. P.; Ghosh, A. K. *Sol. Energy* **1978**, *20*, 443–458.
- (16) Li, S. C.; Diebold, U. *J. Am. Chem. Soc.* **2010**, *132*, 64–66.
- (17) Tanaka, K.; Capule, M. F. V.; Hisanaga, T. *Chem. Phys. Lett.* **1996**, *187*, 73–76.
- (18) Kho, Y. K.; Iwase, A.; Teoh, W. Y.; Mädler, L.; Kudo, A.; Amal, R. *J. Phys. Chem. C* **2010**, *114*, 2821–2829.
- (19) Zachariah, A.; Baiju, K. V.; Shukla, S.; Deepa, K. S.; James, J.; Warriar, K. G. K. *J. Phys. Chem. C* **2008**, *112*, 11345–11356.
- (20) Klosek, S.; Raftery, D. *J. Phys. Chem. B* **2001**, *105*, 2815–2819.
- (21) Choi, W.; Termin, A.; Hoffmann, M. R. *J. Phys. Chem.* **1994**, *98*, 13669–13679.
- (22) Nosaka, Y.; Matushita, M.; Nishino, J.; Nosaka, A. Y. *Sci. Technol. Adv. Mater.* **2005**, *6*, 143–148.
- (23) Asahi, R.; Morikawa, T.; Ohwaki, T.; Aoki, K.; Taga, Y. *Science* **2001**, *293*, 269–271.
- (24) Nonoyama, T.; Tanaka, M.; Kinoshita, T.; Nagata, F.; Sato, K.; Kato, K. *Chem. Commun.* **2010**, *46*, 6983–6985.
- (25) Nonoyama, T.; Kinoshita, T.; Higuchi, M.; Nagata, K.; Tanaka, M.; Sato, K.; Kato, K. *Langmuir* **2011**, *27*, 7077–7083.
- (26) Kuno, T.; Nonoyama, T.; Hirao, K.; Kato, K. *Langmuir* **2011**, *27*, 13154–13158.
- (27) Mann, S. *Nature* **1988**, *332*, 119–124.

- (28) Mann, S.; Ozin, G. A. *Nature* **1996**, *382*, 313–318.
- (29) Sato, K.; Kumagai, Y.; Watari, K.; Tanaka, J. *Langmuir* **2004**, *20*, 2979–2981.
- (30) Dey, A.; Bomans, P. H. H.; Müller, F. A.; Will, J.; Frederik, P. M.; With, G.; Sommerdijk, N. A. J. M. *Nat. Mater.* **2010**, *9*, 1010–1014.
- (31) Zhang, S.; Holmes, T.; Lockshin, C.; Rich, A. *Proc. Natl. Acad. Sci. U.S.A.* **1993**, *90*, 3334–3338.
- (32) Holmes, T. C.; Lacalle, S. D.; Su, X.; Liu, G.; Rich, A. *Proc. Natl. Acad. Sci. U.S.A.* **2000**, *97*, 6728–6733.
- (33) Nonoyama, T.; Tanaka, M.; Inai, Y.; Higuchi, M.; Kinoshita, T. *ACS Nano* **2011**, *5*, 6174–6183.
- (34) Caruso, R. A.; Schattka, J. H.; Greiner, A. *Adv. Mater.* **2001**, *13*, 1577–1579.